



Photon-number entanglement generated by sequential excitation of a two-level atom

Stephen C. Wein^{1,2}✉, Juan C. Loredo^{1,3,4,5}, Maria Maffei², Paul Hilaire^{3,6}, Abdelmounaim Harouri³, Niccolo Somaschi⁷, Aristide Lemaître³, Isabelle Sagnes³, Loïc Lanco^{3,8}, Olivier Krebs^{1,3}, Alexia Auffèves², Christoph Simon¹, Pascale Senellart³ and Carlos Antón-Solanas^{3,9}✉

Entanglement and spontaneous emission are fundamental quantum phenomena that drive many applications of quantum physics. During the spontaneous emission of light from an excited two-level atom, the atom briefly becomes entangled with the photonic field. Here we show that this natural process can be used to produce photon-number entangled states of light distributed in time. By exciting a quantum dot—an artificial two-level atom—with two sequential π -pulses, we generate a photon-number Bell state. We characterize this state using time-resolved intensity and phase correlation measurements. Furthermore, we theoretically show that applying longer sequences of pulses to a two-level atom can produce a series of multi-temporal mode entangled states with properties intrinsically related to the Fibonacci sequence. Our results on photon-number entanglement can be further exploited to generate new states of quantum light with applications in quantum technologies.

Spontaneous emission is a phenomenon where an excited atom will spontaneously decay while emitting light into the vacuum of the electromagnetic field. Owing to its quantum coherent nature, spontaneous emission can preserve quantum properties such as entanglement and superposition. It has been used to prepare and measure atomic superposition states¹, generate atom–atom^{2,3} and atom–photon entanglement^{4–6}, create single photons^{7,8} and produce entangled photonic states by sequentially manipulating atomic systems^{9–11}, as theoretically proposed in refs. ^{12–14}. It is key to developing quantum memories^{15,16} and quantum networks^{17–20}.

As described in the seminal work of Weisskopf and Wigner²¹, entanglement between light and matter naturally occurs during the spontaneous emission process of a two-level atom—an atom consisting of a ground $|g\rangle$ and excited $|e\rangle$ state. Such entanglement lasts only until the spontaneous emission process brings the atom to the ground state and, as such, has not yet been considered as a direct resource for entangled light generation from a two-level system. Here we show that the light–matter entanglement that occurs during spontaneous emission can be controlled to produce photon-number entangled states distributed in the time domain.

Consider a two-level atom with a spontaneous emission lifetime T_1 . A short π -pulse excitation elevates the atom to the excited state $|e\rangle$ at time $t=0$. In the absence of dephasing, at time $t>0$ the light–matter system evolves into the entangled state $\alpha(t)|e\rangle|0\rangle + \beta(t)|g\rangle|1\rangle$, where $\alpha(t) = e^{-t/2T_1}$, $\beta(t) = \sqrt{1 - \alpha(t)^2}$ and $|n\rangle$ is the state of emitted light containing n photons. Spontaneous emission from a two-level atom can thus be interpreted as a two-qubit gate that generates light–matter entanglement.

For $t \gg T_1$, the atom is left in state $|g\rangle$, separable from the temporally coherent single-photon state $|1\rangle$.

Along the temporal profile of the emitted single-photon wavepacket, we can define adjacent early (e) and late (l) time-bin modes separated by a chosen time-bin threshold time T , which corresponds to the second-quantized temporal creation operators \hat{t}_e^\dagger and \hat{t}_l^\dagger in the pulse-mode formalism^{22–24}. In this new time-bin basis, the pure single-photon state is now written as $|1\rangle = (\alpha(T)\hat{t}_l^\dagger + \beta(T)\hat{t}_e^\dagger)|0\rangle = \alpha(T)|0\rangle_e|1\rangle_l + \beta(T)|1\rangle_e|0\rangle_l$. Note that by choosing T to be the half-life of the source $T_{1/2} = \ln(2)T_1$, the single-photon state is the photon-number Bell state $|\psi^+\rangle = (|01\rangle + |10\rangle)/\sqrt{2}$ (refs. ^{25,26}), where we have concatenated the time-bins and dropped the subscripts for simplicity (Fig. 1a). By extension, a single-photon state could also be expressed as an N -mode W state²⁷ by conveniently defining N time-bin modes.

Now consider the application of a second π -pulse at Δt after the initial pulse, while the atom is still entangled with the field. This second pulse performs a single qubit gate by coherently flipping the state of the atom so that, if a single photon was already emitted before Δt , it will emit a second photon after Δt (Fig. 1b). Conversely, if no photon was emitted before the second pulse, then the atom is brought back to the ground state, preventing any emission from occurring. At Δt just after the second pulse, the total light–matter system is left in the entangled state $\alpha(\Delta t)|g\rangle|0\rangle + \beta(\Delta t)|e\rangle|1\rangle$. Hence, after emission has finished, the emitted photonic state becomes $(\alpha + \beta\hat{t}_e^\dagger\hat{t}_l^\dagger)|0\rangle = \alpha|0\rangle_e|0\rangle_l + \beta|1\rangle_e|1\rangle_l$, as written in the photon number basis for time-bins defined by a T corresponding to the arrival of the second pulse $T = \Delta t$. Consequently, for $T = \Delta t = T_{1/2}$, the emitted photonic state is $|\phi^+\rangle = (|00\rangle + |11\rangle)/\sqrt{2}$. This simple approach can be scaled up to generate multimode entangled photonic states using multiple π -pulses, as discussed later on.

¹Institute for Quantum Science and Technology and Department of Physics and Astronomy, University of Calgary, Calgary, Alberta, Canada. ²Université Grenoble Alpes, CNRS, Grenoble INP, Institut Néel, Grenoble, France. ³Centre for Nanosciences and Nanotechnology, CNRS, Université Paris-Saclay, UMR 9001, Palaiseau, France. ⁴University of Vienna, Faculty of Physics, Vienna Center for Quantum Science and Technology (VCQ), Vienna, Austria.

⁵Christian Doppler Laboratory for Photonic Quantum Computer, Faculty of Physics, University of Vienna, Vienna, Austria. ⁶Department of Physics, Virginia Tech, Blacksburg, VA, USA. ⁷Quandela SAS, Palaiseau, France. ⁸Université Paris Cité, Centre de Nanosciences et Nanotechnologies, Palaiseau, France.

⁹Institute of Physics, Carl von Ossietzky University, Oldenburg, Germany. ✉e-mail: wein.stephen@gmail.com; c.anton.so@gmail.com

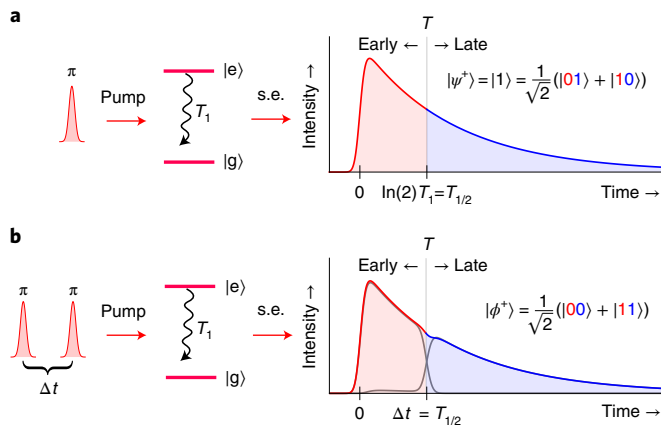


Fig. 1 | Generation of photon-number Bell states. **a**, A single photon is produced by spontaneous emission (s.e.) after a single π -pulse excitation of a two-level atom with a lifetime of T_1 . Partitioning this photon into two orthogonal time-bins (early and late), which are defined by setting T to $T_{1/2} = \ln(2)T_1$, reveals $|\psi^+\rangle$. **b**, Applying a subsequent π -pulse after $\Delta t = T_{1/2}$ flips the state of the two-level atom while it is entangled with the photon field. By choosing T to coincide with the second pulse, we find $|\phi^+\rangle$.

Results

We experimentally explore this scheme using a single semiconductor quantum dot acting as an artificial atom. The quantum dot is coupled to a micropillar cavity mode operating far into the bad-cavity regime²⁸ in which emission into the cavity mode is irreversible. The device studied here consists of a negatively charged exciton addressed resonantly in a cross-polarized collection set-up²⁹ so that the optical transition, which has a measured lifetime of $T_1 = 136 \pm 1$ ps, is modelled as a resonantly driven two-level atom. The laser excitation pulses are typically ten times shorter than the spontaneous emission lifetime of the transition and Rabi oscillations are observed as a function of the pulse power, attesting the coherent control of the device³⁰.

The single-photon nature of emission from the device is characterized by measuring a second-order correlation of $g^{(2)}(0) = 0.063 \pm 0.002$ ($g^{(2)}$ for simplicity) after integrating over the pulsed emission following a single π -pulse excitation, and normalizing by the uncorrelated coincident counts at long delay times $g_\tau^{(2)} > g^{(2)}$. The coherent light-matter interaction during spontaneous emission is exemplified by the observation of Hong–Ou–Mandel (HOM) bunching^{31,32} between successively emitted single-photons interfering at a beam splitter. We measure a correlation of $g_{\text{HOM}}^{(2)} = 0.145 \pm 0.004$ at the output, which attests to the low probability of two photons exiting the beam splitter separately. These measurements together provide a mean wavepacket overlap of $M = 1 - 2g_{\text{HOM}}^{(2)} + g^{(2)} = 0.77 \pm 0.01$ and an estimated single-photon indistinguishability $M_s = M/(1-g^{(2)}) = 0.82 \pm 0.02$ at the source³³.

The indistinguishability of a single-photon wavepacket characterizes how coherent it is in time; $|\psi^+\rangle$ is also strongly linked to this same temporal coherence, being a superposition of states $|01\rangle$ and $|10\rangle$ of a photon arriving in two different time-bins. In the Supplementary Information, we theoretically show and experimentally verify that the Bell-state fidelity of a single photon with respect to $|\psi^+\rangle$ is well-approximated by $\mathcal{F}_{\psi^+} \simeq p_1 \sqrt{M_s} = 0.88 \pm 0.02$ when choosing $T = T_{1/2} = 94$ ps, where p_1 is the probability of emitting a single photon. Here we proceed to experimentally explore the proposed scheme to generate $|\phi^+\rangle$ by applying a second π -pulse separated from the first by the half-life $\Delta t \simeq T_{1/2}$.

The ideal $|\phi^+\rangle$ state comprises two photons, each with a probability of $p_2 = 1/2$, and a vacuum ($p_0 = 1/2$). This renders an expected

intensity correlation of $g^{(2)} = 1$ and an average photon number of $\mu = 1$ at the source. We confirm this prediction by measuring $g^{(2)} = 0.99 \pm 0.02$ and $\mu/\mu_\pi = 1.02 \pm 0.01$ with respect to the average photon number μ_π produced by a single pulse, which is expected to be near unity at the source. We also verify that producing three or more photons is rare by measuring a small third-order correlation $g^{(3)} = 0.165 \pm 0.007$, which corresponds to a three-photon emission probability of about 3% (a detailed discussion on photon number probabilities and losses is given in the Supplementary Information). The photon statistics thus already suggest a state of the form $|0\rangle + |2\rangle$. It remains now to demonstrate a separation of the two photons into early and late time-bins $|11\rangle$, and the presence of coherence with the vacuum part of the state $|00\rangle$.

To access temporal properties after the application of two pulses, we first measure the temporal profile and find that it matches well with the profile produced after excitation by a single π -pulse (Fig. 2a), as foreshadowed by Fig. 1. By sweeping T across the wavepacket, we find that the proportion of counts $\bar{\mu}_a = \mu_a/\mu$ detected in each time-bin $a \in \{e, l\}$ cross at the half-life condition (Fig. 2b). This matches the trend given by the ideal $|\phi^+\rangle$.

We study the two photons composing the total temporal profile by performing time-resolved intensity correlation measurements (Methods). This produces a two-time coincidence map $G^{(2)}(t_1, t_2)$ that can be divided into four time-bin quadrants defined by a chosen T , designated ee, el, le and ll as shown in Fig. 2c. The direct inspection of this map reveals that coincident counts between different time-bins (el, le) predominantly occur when $T = \Delta t \simeq T_{1/2}$, indicating that the two photons are indeed temporally separated.

To quantify this observation, we analyse each quadrant of the $G^{(2)}$ map individually. The counts in each quadrant are summed and normalized by the product of average photon numbers $\mu_a \mu_b$ obtained within each pair of bins $a, b \in \{e, l\}$. This gives the normalized correlation $g_{ab}^{(2)}$ for the pair of time-bins where a coincidence count was detected. The total $g^{(2)}$ is then seen as an average of each $g_{ab}^{(2)}$ weighted by the proportion $\bar{\mu}_a \bar{\mu}_b$.

The time-bin analysis of $g^{(2)}$ presented in Fig. 2d reveals that anti-bunching occurs for detection within the same bins ($g_{ee}^{(2)}, g_{ll}^{(2)} < 1$), whereas bunching occurs between different bins ($g_{el}^{(2)} = g_{le}^{(2)} > 1$). Bunching is maximum when the time-bin threshold is chosen at the half-life; however, the amount of bunching is less than would be expected from an ideal state produced by infinitesimally short pulses and measured with perfect time resolution (dashed curves). This is primarily due to the detection time jitter (Methods), which occasionally detects photons in quadrants ee and ll that would otherwise reside in el or le, and hence decreases $g_{el}^{(2)}$ while increasing $g_{ee}^{(2)}$ and $g_{ll}^{(2)}$. From this intensity correlation analysis, we find that $81.5 \pm 0.4\%$ of two-photon measurements occur in different time-bins, evidencing a primary $|11\rangle$ component. We now probe the expected coherent properties of the photonic state using phase correlation measurements.

The intensity correlation $g_{\text{HOM}}^{(2)}$ at the output of a path-unbalanced Mach–Zehnder interferometer—commonly used to measure HOM bunching—can oscillate as the interferometer phase ϕ evolves. This occurs when the input contains coherence between any states that differ by two photons (second-order coherence). We recently used this technique to measure the amount of coherence generated between the vacuum and two photons when exciting a two-level atom with a single 2π -pulse³⁴. We use this same concept to characterize the number coherence generated after applying sequential π -pulses by interfering two of the generated photonic states (Fig. 3a).

The correlation $g_{\text{HOM}}^{(2)}$ depends on both $g^{(2)}$ and the mean wavepacket overlap M (ref. ³³). By considering photon-number coherence, a phase-dependent term arises³⁵:

$$2g_{\text{HOM}}^{(2)}(\phi) = 1 - M + g^{(2)} - c^{(2)} \cos(2\phi), \quad (1)$$

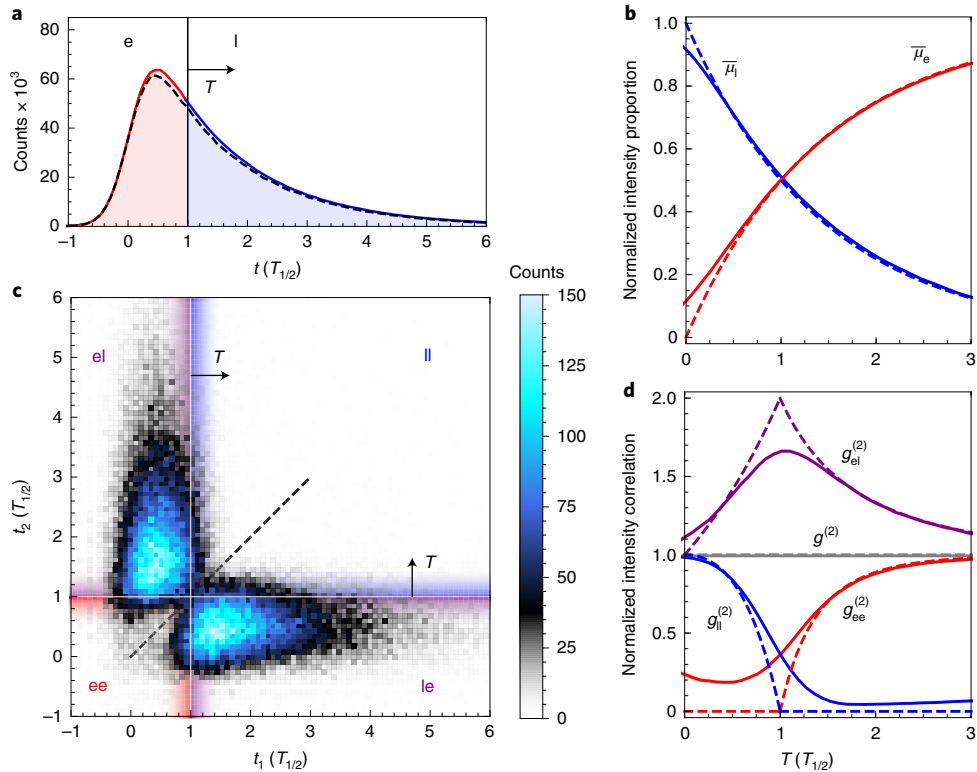


Fig. 2 | Characterization of intensity. **a**, The temporal profile measured after applying two π -pulses separated in time by the half-life $\Delta t \simeq T_{1/2}$. The profile is divided into early and late bins defined by the T . The black dashed line shows the single-photon profile obtained for the same measurement duration after applying a single π -pulse. **b**, The normalized proportion of counts detected in the early $\bar{\mu}_e$ and late $\bar{\mu}_l$ time-bins as T is swept over the temporal profile. **c**, The time-resolved intensity correlation map $G^{(2)}(t_1, t_2)$ divided by T into four quadrants corresponding to each pair of time-bins where a coincidence detection occurs. **d**, The intensity correlation for each quadrant $g_{ab}^{(2)}$ normalized by the square average photon number $\mu_a \mu_b$ detected in bins $a, b \in \{e, l\}$, computed from **c** as T is swept across the wavepacket. We obtain $g_{el}^{(2)} = g_{le}^{(2)}$ by averaging the counts in the off-diagonal quadrants. The dashed curves in **b** and **d** show the values expected for an ideal $|\phi^+\rangle$. The solid curves show the measured values where the standard uncertainty is smaller than the thickness of the line.

where $c^{(2)}$ is an intensity-normalized value quantifying the second-order coherence, as described in the Supplementary Information. In our set-up, ϕ freely evolves on a slow timescale (Methods). To accurately extract $c^{(2)}$, we simultaneously monitor the self-homodyne signal $I_{SH} = (\mu^+ - \mu^-)/\mu \propto \cos(\phi)$, which is the normalized difference in average photon number μ^\pm detected at each output. As $g_{HOM}^{(2)}$ and I_{SH} depend on the phase through $-\cos(2\phi)$ and $\cos(\phi)$, respectively, we expect a quadratic phase-correlated parametric relationship $g_{HOM}^{(2)} \approx -I_{SH}^2$, with an amplitude of $c^{(2)}$.

Although an ideal $|\phi^+\rangle$ should give $I_{SH}=0$, as it does not have first-order coherence³⁴, the finite temporal width of pulses applied to the atom inevitably cause a small signal $|I_{SH}| \ll 1$. We believe this signal is produced by the atom directly when a photon is occasionally emitted during the excitation pulse, which allows for the remainder of the pulse to prepare the atom in a superposition state; however, it could also arise from over/underestimating the π -pulse conditions or from imperfect polarization filtering of the excitation pulses. By monitoring this remnant self-homodyne signal, we observe the expected quadratic signature and use it to measure $c^{(2)}$ for three different pulse separations Δt (Fig. 3b). The amplitude of oscillation increases with decreasing Δt due to normalizing by intensity, hence illustrates a convergence toward the vacuum. A full analysis and discussion of measurements when varying Δt is available in the Supplementary Information. The total time-integrated value $c^{(2)}$ indicates substantial second-order coherence, but it does not distinguish states of the form $|0\rangle + |2\rangle$ from $|00\rangle + |11\rangle$. For this, we resolve the measurement in time.

Consider the interference of two ideal Bell states (Fig. 3a). This gives rise to four cases. First, the vacuum inputs $|00\rangle$ will give a trivial output. Second, two $|11\rangle$ states will cause HOM bunching (Fig. 3c). As opposed to the ideal single-photon case in which $M=1$, an ideal $|\phi^+\rangle$ should give $M=1/2$. This is as both early and late photons bunch with their pair in the same time-bin ($M_{ee}=M_{ll}=1$), but each pair can still exit the beam splitter independently ($M_{el}=M_{le}=0$). Third, the cases combining $|00\rangle$ and $|11\rangle$ can occur in two ways (Fig. 3d). If cases two and three produce indistinguishable outputs, then a quantum interference occurs due to the erasure of the information about which path the two photons took through the interferometer. This two-photon interference evidences the presence of a path-entangled Bell state between the upper U and lower L paths of the interferometer: $(|U\rangle_e|U\rangle_l + e^{2i\phi}|L\rangle_e|L\rangle_l)/\sqrt{2}$, and it causes an oscillation of coincident counts depending on ϕ that contributes to the $c^{(2)}$ term of $g_{HOM}^{(2)}$. Thus, monitoring the oscillation of coincidence counts constitutes a Bell-state measurement of this path-entangled state produced by the $|\phi^+\rangle$ input; however, to distinguish $|\phi^+\rangle$ from arbitrary states of the form $|0\rangle + |2\rangle$, we must measure the component of $c_{el(le)}^{(2)}$ that arises from coincidences between photons arriving in different time-bins and show that it exceeds any contribution from $c_{ee(ll)}^{(2)}$.

To measure M_{ab} and $c_{ab}^{(2)}$, we use the same approach used to obtain $g_{ab}^{(2)}$, by analysing each quadrant of the time-resolved correlation map $G_{HOM}^{(2)}(t_1, t_2, \phi)$ for a given T . We subdivide each map $G_{HOM}^{(2)}(t_1, t_2, \phi)$ corresponding to each $I_{SH}(\phi)$, which produces four quadratic signatures similar to those presented in Fig. 3b, with one

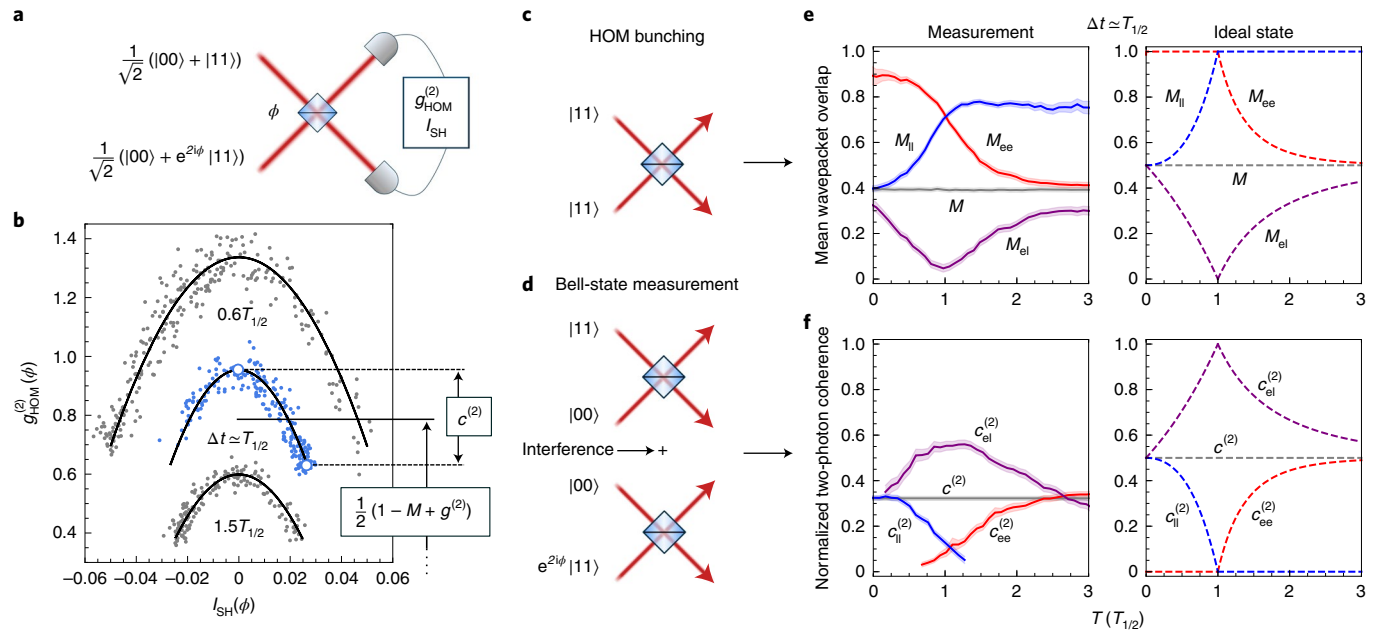


Fig. 3 | Characterization of coherence. **a**, Two ideal Bell states interfering at a beamsplitter, after which the normalized $g_{\text{HOM}}^{(2)}$ and self-homodyne signal I_{SH} are measured. **b**, The fitted quadratic relationship (black curve) between the coincidence counts ($g_{\text{HOM}}^{(2)}(\phi)$) and the detection rate difference ($I_{\text{SH}}(\phi)$) for three different pulse separations Δt (see labels, data for $1.5T_{1/2}$ are shifted down by 0.2 for clarity). Each data point in this panel is computed by integrating over the entire time-resolved correlation map $G_{\text{HOM}}^{(2)}(t_1, t_2, \phi)$ for a given measured $I_{\text{SH}}(\phi)$. **c**, Sketch of the HOM bunching case when interfering two $|11\rangle$ states. **d**, Sketch of the path-entangled Bell state interference. **e,f**, The mean wavepacket overlaps M_{ab} (**e**) and normalized second-order coherence magnitudes $c_{ab}^{(2)}$ (**f**) for time-bins $a, b \in \{\text{e}, \text{l}\}$. These quantities are extracted as in **b** but using instead $g_{\text{HOM}, ab}^{(2)}(\phi)$ obtained by integrating and normalizing $G_{\text{HOM}}^{(2)}(t_1, t_2, \phi)$ for each quadrant, as was done for $G^{(2)}(t_1, t_2)$ to obtain $g_{ab}^{(2)}$ in Fig. 2. The shaded regions show the standard uncertainty obtained from fitting the scattered data. For clarity, we show separate panels for the values expected for an ideal $|\phi^+\rangle$ (dashed curves).

corresponding to each quadrant. We then fit these four sets of data to extract the quantities $c_{ab}^{(2)}$ and M_{ab} .

From the time-bin analysis of phase correlations, we see that the mean wavepacket overlaps of photons in the same bins M_{ee} and M_{ll} both remain relatively high and intersect at the half-life, whereas the overlap between bins M_{el} dips nearly to zero (Fig. 3e). This indicates that the photons composing $|11\rangle$ are mostly individually indistinguishable, yet almost fully distinguishable from each other. Interestingly, M_{ee} exceeds the mean wavepacket overlap measured after a single π -pulse ($M \approx 0.77$) when $T < T_{1/2}$. We attribute this to the sharp temporal truncation of photons in the early bin, which causes a spectral broadening that partially overcomes dephasing. This truncation does not modify the temporal shape of photons in the late bin, which remain as exponentially decaying profiles. Hence, M_{ll} converges to the single-photon case when $T > T_{1/2}$. The observed crossing and dip follows that predicted by the ideal state and verifies the scenario described by Fig. 3c when $T = T_{1/2}$.

We find that the trend for $c_{ab}^{(2)}$ mimics that of $g_{ab}^{(2)}$, as predicted by the ideal state, with $c_{el}^{(2)}$ peaking when $c_{ee}^{(2)}$ and $c_{ll}^{(2)}$ intersect at the half-life (Fig. 3f); however, the magnitudes are further suppressed relative to the ideal case as the coherence is susceptible to dephasing in addition to errors caused by imperfect pulses and detection jitter. That said, we find that $c_{el}^{(2)}$ is much greater than $c_{ee}^{(2)}$ and $c_{ll}^{(2)}$ at the half-life, indicating that the majority of the oscillation observed in $g_{\text{HOM}}^{(2)}$ arises from a coherence between the vacuum $|00\rangle$ and two photons arriving in orthogonal time-bins $|11\rangle$.

The three intensity-normalized quantities $c_{el}^{(2)}$, M_{ee} and M_{ll} can be used to estimate the magnitude of some density matrix elements of the photonic state at the source, before losses from collection. From this, we estimate that the emitted state has an entanglement concurrence of $C = 0.70 \pm 0.05$. Note that a positive value $C > 0$ unambiguously indicates the presence of quantum entanglement³⁶. We also estimate a fidelity of $\mathcal{F}_{\phi^+} = 0.79 \pm 0.03$ with respect to $|\phi^+\rangle$.

biguously indicates the presence of quantum entanglement³⁶. We also estimate a fidelity of $\mathcal{F}_{\phi^+} = 0.79 \pm 0.03$ with respect to $|\phi^+\rangle$.

Discussion

Our fidelity and concurrence estimates are limited by the detector jitter time. The measurements of $c^{(2)}$ and M suggest that a fidelity up to 0.86 is possible with this device using detectors with a time jitter well below³⁷ the pulse timescale ($t_p = 20$ ps) used in our experiments, which would reduce the proportion of two-photon events occurring within the same time-bins (ee or ll) down to $3t_p/8T_1 \approx 5\%$ (Supplementary Information). Using shorter pulses ($t_p \ll T_1$) in combination with low time-jitter detectors would bring the fidelity up to at most $\sqrt{M_s} \approx 0.91$, which is limited by the dephasing of this device. Note that $M_s \geq 0.975$ has been achieved with quantum dot devices^{38,39}, which could provide a fidelity of up to 0.987.

In our experiments we do not perform a full quantum state tomography on the photonic state to retrieve its density matrix as it is difficult to spatially separate and independently analyse the time-bin modes. We instead characterize the photon-number entanglement of the state via intensity and phase correlation measurements, which, under some reasonable assumptions, allows for a partial reconstruction of the density matrix and for estimates of fidelity and concurrence (Supplementary Information). One approach to separate the time-bins would be to use an ultrafast optical switch; this would in turn allow for single-qubit gates, quantum teleportation and Bell tests. For our system, the short lifetime dictates an optical switching time on the picosecond timescale, which is achievable using lithium niobate integrated photonic circuits⁴⁰; however, our approach for generating photonic entanglement can be applied to any coherently controlled source of indistinguishable photons modelled by a two-level system.

Our entangling protocol also has a simple extension to multi-mode entanglement by applying a longer sequence of π -pulses. As detailed in the Supplementary Information, the photonic state $|\psi_N\rangle$ produced by N pulses has a recursive nature that becomes transparent when labelling the time-bins in reverse chronological order. In this case, by applying the matrix product state formalism^{13,14}, we find that the final state can be determined from the Fibonacci-like relation

$$|\psi_N\rangle = \alpha_N |\psi_{N-2}\rangle + \beta_N \hat{t}_N^\dagger |\psi_{N-1}\rangle, \quad (2)$$

where $\alpha_m = e^{-\Delta t_m/2T_1}$, $\beta_m = \sqrt{1 - \alpha_m^2}$, $\hat{t}_m^\dagger |0\rangle_m = |1\rangle_m$, and where m labels the m th time-bin from the end of the sequence. If $\Delta t_1 \gg T_1$ so that the atom relaxes to the ground state at the end of the sequence, then $N=1$ pulse produces a single photon $|\psi_1\rangle = |1\rangle_1$ and $N=2$ pulses produces the entangled state: $|\psi_2\rangle = \alpha_2 |0\rangle_2 |0\rangle_1 + \beta_2 |1\rangle_2 |1\rangle_1$. By choosing the pulse separations $\Delta t_2 = T_1 \ln(2)$ and $\Delta t_3 = T_1 \ln(3)$, we obtain the maximally entangled W -class state produced by $N=3$ pulses: $|\psi_3\rangle = (|001\rangle + |100\rangle + |111\rangle)/\sqrt{3}$. In general, the entangled states produced by this sequence belong to the class of matrix product states with two-dimensional bonds^{13,14}, and they are not equivalent to N -qubit W states for $N \geq 4$. Further studies are needed to identify the type and amount of entanglement provided by multi-pulse sequences applied to two-level atoms.

Conclusion

We have shown that the light-matter entanglement occurring during spontaneous emission from a two-level atom is a fundamental resource for generating entangled light. By probing the temporal domain of pulsed light emitted by an artificial atom after a double π -pulse excitation, our measurements demonstrate the generation of a photon-number Bell state. By adding more consecutive π -pulses, we herald that this protocol can produce multipartite temporal entanglement, and it is a step closer to the generation of high-order Fock states and cat states, which require dynamic control of the light-matter coupling strength^{41–43}. Such a new class of photonic states could serve as building blocks for distributing entanglement, quantum state teleportation, and may allow new ways to implement quantum random walks, quantum sensing and photonic networks⁴⁴. We also believe that the sequential coherent driving of multi-level atomic systems during spontaneous emission offers promising perspectives for generating high-dimensional entanglement⁴⁵; for example, using the biexciton-exciton cascade in semiconductor quantum dots or in combination with spin-photon entanglement protocols.

Online content

Any methods, additional references, Nature Research reporting summaries, source data, extended data, supplementary information, acknowledgements, peer review information; details of author contributions and competing interests; and statements of data and code availability are available at <https://doi.org/10.1038/s41566-022-00979-z>.

Received: 4 June 2021; Accepted: 16 February 2022;

Published online: 7 April 2022

References

- Monroe, C., Meekhof, D. M., King, B. E. & Wineland, D. J. A “Schrödinger cat” superposition state of an atom. *Science* **272**, 1131–1136 (1996).
- Ritter, S. et al. An elementary quantum network of single atoms in optical cavities. *Nature* **484**, 195–200 (2012).
- Slodička, L. et al. Atom–atom entanglement by single-photon detection. *Phys. Rev. Lett.* **110**, 083603 (2013).
- Blinov, B. B., Moehring, D. L., Duan, L. M. & Monroe, C. Observation of entanglement between a single trapped atom and a single photon. *Nature* **428**, 153–157 (2004).
- Wilk, T., Webster, S. C., Kuhn, A. & Rempe, G. Single-atom single-photon quantum interface. *Science* **317**, 488–490 (2007).
- De Greve, K. et al. Quantum-dot spin–photon entanglement via frequency downconversion to telecom wavelength. *Nature* **491**, 421–425 (2012).
- Brunel, C., Lounis, B., Tamarat, P. & Orrit, M. Triggered source of single photons based on controlled single molecule fluorescence. *Phys. Rev. Lett.* **83**, 2722–2725 (1999).
- Michler, P. A quantum dot single-photon turnstile device. *Science* **290**, 2282–2285 (2000).
- Neumann, P. et al. multipartite entanglement among single spins in diamond. *Science* **320**, 1326–1329 (2008).
- Schwartz, I. et al. Deterministic generation of a cluster state of entangled photons. *Science* **354**, 434–437 (2016).
- Besse, J.-C. et al. Realizing a deterministic source of multipartite-entangled photonic qubits. *Nat. Commun.* **11**, 4877 (2020).
- Saavedra, C., Gheri, K. M., Törmä, P., Cirac, J. I. & Zoller, P. Controlled source of entangled photonic qubits. *Phys. Rev. A* **61**, 062311 (2000).
- Schön, C., Solano, E., Verstraete, F., Cirac, J. I. & Wolf, M. M. Sequential generation of entangled multiqubit states. *Phys. Rev. Lett.* **95**, 110503 (2005).
- Schön, C., Hammerer, K., Wolf, M. M., Cirac, J. I. & Solano, E. Sequential generation of matrix-product states in cavity QED. *Phys. Rev. A* **75**, 032311 (2007).
- Maître, X. et al. Quantum memory with a single photon in a cavity. *Phys. Rev. Lett.* **79**, 769–772 (1997).
- Specht, H. P. et al. A single-atom quantum memory. *Nature* **473**, 190–193 (2011).
- Cirac, J. I., Zoller, P., Kimble, H. J. & Mabuchi, H. Quantum state transfer and entanglement distribution among distant nodes in a quantum network. *Phys. Rev. Lett.* **78**, 3221–3224 (1997).
- Chou, C.-W. et al. Functional quantum nodes for entanglement distribution over scalable quantum networks. *Science* **316**, 1316–1320 (2007).
- Yuan, Z.-S. et al. Experimental demonstration of a BDCZ quantum repeater node. *Nature* **454**, 1098–1101 (2008).
- Daiss, S. et al. A quantum-logic gate between distant quantum-network modules. *Science* **371**, 614–617 (2021).
- Weisskopf, V. & Wigner, E. Berechnung der natürlichen linienbreite auf Grund der diracschen lichttheorie. *Zeit. Phys.* **63**, 54–73 (1930).
- Blow, K. J., Loudon, R., Phoenix, S. J. D. & Shepherd, T. J. Continuum fields in quantum optics. *Phys. Rev. A* **42**, 4102–4114 (1990).
- Hussain, N., Imoto, N. & Loudon, R. Quantum theory of dynamic interference experiments. *Phys. Rev. A* **45**, 1987–1996 (1992).
- Özdemir, Ş. K., Miranowicz, A., Koashi, M. & Imoto, N. Pulse-mode quantum projection synthesis: effects of mode mismatch on optical state truncation and preparation. *Phys. Rev. A* **66**, 053809 (2002).
- Van Enk, S. J. Single-particle entanglement. *Phys. Rev. A* **72**, 064306 (2005).
- Specht, H. P. et al. Phase shaping of single-photon wave packets. *Nat. Photon.* **3**, 469–472 (2009).
- Dür, W., Vidal, G. & Cirac, J. I. Three qubits can be entangled in two inequivalent ways. *Phys. Rev. A* **62**, 062314 (2000).
- Hilaire, P. et al. Deterministic assembly of a charged-quantum-dot-micropillar cavity device. *Phys. Rev. B* **102**, 195402 (2020).
- Kuhlmann, A. V. et al. A dark-field microscope for background-free detection of resonance fluorescence from single semiconductor quantum dots operating in a set-and-forget mode. *Rev. Sci. Instrum.* **84**, 073905 (2013).
- Stievater, T. H. et al. Rabi oscillations of excitons in single quantum dots. *Phys. Rev. Lett.* **87**, 133603 (2001).
- Hong, C. K., Ou, Z. Y. & Mandel, L. Measurement of subpicosecond time intervals between two photons by interference. *Phys. Rev. Lett.* **59**, 2044–2046 (1987).
- Kiraz, A., Atatüre, M. & İmamoğlu, A. Quantum-dot single-photon sources: prospects for applications in linear optics quantum-information processing. *Phys. Rev. A* **69**, 032305 (2004).
- Ollivier, H. et al. Hong-Ou-mandel interference with imperfect single photon sources. *Phys. Rev. Lett.* **126**, 063602 (2021).
- Loredo, J. C. et al. Generation of non-classical light in a photon-number superposition. *Nat. Photon.* **13**, 803–808 (2019).
- Wein, S. C. *Modelling Markovian Light–Matter Interactions for Quantum Optical Devices in the Solid State*. PhD thesis, Univ. Calgary (2021).
- Wootters, W. K. Entanglement of formation and concurrence. *Quantum Inf. Comput.* **1**, 27–44 (2001).
- Korzh, B. et al. Demonstration of sub-3 ps temporal resolution with a superconducting nanowire single-photon detector. *Nat. Photon.* **14**, 250–255 (2020).
- Somaschi, N. et al. Near-optimal single-photon sources in the solid state. *Nat. Photon.* **10**, 340–345 (2016).
- Tomm, N. et al. A bright and fast source of coherent single photons. *Nat. Nanotechnol.* **16**, 399–403 (2021).

40. Wang, C. et al. Integrated lithium niobate electro-optic modulators operating at CMOS-compatible voltages. *Nature* **562**, 101–104 (2018).
41. Law, C. K. & Eberly, J. H. Arbitrary control of a quantum electromagnetic field. *Phys. Rev. Lett.* **76**, 1055–1058 (1996).
42. Cosacchi, M. et al. On-demand generation of higher-order fock states in quantum-dot-cavity systems. *Phys. Rev. Res.* **2**, 033489 (2020).
43. Cosacchi, M. et al. Schrödinger cat states in quantum-dot-cavity systems. *Phys. Rev. Res.* **3**, 023088 (2021).
44. Briegel, H. J. & Raussendorf, R. Persistent entanglement in arrays of interacting particles. *Phys. Rev. Lett.* **86**, 910–913 (2001).
45. Erhard, M., Krenn, M. & Zeilinger, A. Advances in high-dimensional quantum entanglement. *Nat. Rev. Phys.* **2**, 365–381 (2020).

Publisher's note Springer Nature remains neutral with regard to jurisdictional claims in published maps and institutional affiliations.

© The Author(s), under exclusive licence to Springer Nature Limited 2022

Methods

More details about the quantum-dot-micropillar source used in our experiments can be found in ref.⁴⁶, source number 3, following the numbering of this reference. This source was chosen over others for its very high emission efficiency, which allows for fast collection of time-resolved maps and third-order intensity correlations. The experiments were performed in a standard resonant cross-polarization set-up^{46–48}. We prepare the two- π -pulse sequence in a compact Michelson interferometer. This provides passive phase-stabilization for the delayed output pulses and independent intensity tuning. One of the mirrors is mounted on a nanometric translation stage allowing for delay tuning of up to 175 ps. The laser pulses have a temporal full-width at half-maximum of ~20 ps. The coincidence maps are retrieved via time-tagging of the photon events with respect to the laser clock⁴⁹. The phase correlation measurements are implemented in a path unbalanced Mach-Zehnder interferometer, with a delay of 12.3 ns in one of the arms, matching the laser repetition rate⁴⁸. The ϕ of the interferometer evolves slowly, performing a π shift on the ~5 s timescale. The relatively fast 100 ms time to acquire a single time-resolved correlation map $G_{\text{HOM}}^{(2)}(t_1, t_2, \phi)$ allows us to consider the ϕ constant for each map.

The device and set-up losses are detailed in refs.^{46,50}. The probability of having a single photon per pulsed excitation in the collection single-mode fibre is ~10%. All measurements are performed using superconducting nanowire single-photon detectors with ~70% quantum efficiency and ~50 ps full-width at half-maximum Gaussian jitter time. The $g^{(3)}$ and $g_{\text{HOM}}^{(2)}$ measurements are intensity-normalized quantities that are insensitive to photon losses, thus allowing characterization of the photonic state at the source level before any photon collection, transmission and detection losses. Under a single π -pulse excitation, the count rate per detector in the intensity correlation measurements ($g^{(3)}$ Hanbury-Brown-Twiss set-up, with three detectors) is 1.256 ± 0.007 MHz per detector, and the count rate per detector for the $g_{\text{HOM}}^{(2)}$ coherence measurements (output of the Mach-Zehnder interferometer) is 0.899 ± 0.005 MHz per detector. The photon time-tags are processed in a HydraHarp 400 autocorrelator, with a temporal discretisation of 8 ps.

Data availability

The experimental data that support the findings of this study are available in figshare at <https://doi.org/10.6084/m9.figshare.16838248>.

References

46. Ollivier, H. et al. Reproducibility of high-performance quantum dot single-photon sources. *ACS Photon.* **7**, 1050–1059 (2020).
47. Kuhlmann, A. V. et al. A dark-field microscope for background-free detection of resonance fluorescence from single semiconductor quantum dots operating in a set-and-forget mode. *Rev. Sci. Instrum.* **84**, 073905 (2013).
48. Loredo, J. C. et al. Generation of non-classical light in a photon-number superposition. *Nat. Photon.* **13**, 803–808 (2019).
49. Flagg, E. B., Polyakov, S. V., Thomay, T. & Solomon, G. S. Dynamics of nonclassical light from a single solid-state quantum emitter. *Phys. Rev. Lett.* **109**, 163601 (2012).
50. Hilaire, P. et al. Deterministic assembly of a charged-quantum-dot-micropillar cavity device. *Phys. Rev. B* **102**, 195402 (2020).

Acknowledgements

P.S. acknowledges support from the ERC PoC PhoW, the IAD—ANR support ASTRID programme project (grant no. ANR-18-ASTR-0024 LIGHT), the QuantERA ERA-NET Cofund in Quantum Technologies (project HIPHOP), the FET OPEN QLUSTER, and the French RENATECH network, a public grant overseen by the French National Research Agency (ANR) as part of the Investissements d'Avenir programme (Labex NanoSaclay, grant no. ANR-10-LABX-0035). J.C.L. acknowledges the Austrian Federal Ministry for Digital and Economic Affairs, the National Foundation for Research, Technology and Development, and the Christian Doppler Research Association. A.A., M.M. and S.C.W. acknowledge support from the Foundational Questions Institute Fund (grant no. FQXi-IAF19-01 to A.A. and S.C.W., and FQXi-IAF19-05 to A.A. and M.M.), as well as the European Union's Horizon 2020 research and innovation programme under the Marie Skłodowska-Curie (grant agreement no. 861097 to A.A., M.M. and S.C.W.). A.A. and M.M. also acknowledge support from the ANR Research Collaborative Project Qu-DICE (grant no. ANR-PRC-CES47 to A.A and M.M.), the Templeton World Charity Foundation Inc (grant no. TWCF0338 to A.A. and M.M.) and the John Templeton Foundation (grant no. 61835 to A.A.). C.S. acknowledges support from the Natural Sciences and Engineering Research Council of Canada (NSERC) Discovery Grant and Strategic Project Grant programs, as well as the National Research Council's High-Throughput Secure Networks program. S.C.W. also acknowledges support from the NSERC Canadian Graduate Scholarships (grant nos 668347 and 677972) and the SPIE Education Scholarship program. S.C.W. and C.A.-S. acknowledge A. González-Tudela, C. Sánchez-Muñoz, T. Huber and N. Sinclair for fruitful discussions. C.A.-S. thanks K. Bencheikh and F. Raineri for providing technical assistance in the experimental set-up.

Author contributions

The experiments were conducted by J.C.L. and C.A.-S. Data analysis was carried out by S.C.W. and C.A.-S. with help from J.C.L. and P.H. Theoretical modelling was performed by S.C.W., M.M., C.S. and A.A., with help from J.C.L and C.A.-S.. Cavity devices were fabricated by A.H. and N.S. from samples grown by A.L. based on a design of L.L. Etching was performed by I.S. The manuscript was written by S.C.W. and C.A.-S. with assistance from C.S. and P.S. and input from all authors. The project was supervised by C.A.-S. with the collaboration of C.S. and P.S.

Competing interests

N.S. is a co-founder—and P.S. is a scientific advisor and co-founder—of the single-photon-source company Quandela. The other authors declare no competing interests.

Additional information

Supplementary information The online version contains supplementary material available at <https://doi.org/10.1038/s41566-022-00979-z>.

Correspondence and requests for materials should be addressed to Stephen C. Wein or Carlos Antón-Solanas.

Peer review information *Nature Photonics* thanks Adam Miranowicz, Tracy Northup and the other, anonymous, reviewer(s) for their contribution to the peer review of this work.

Reprints and permissions information is available at www.nature.com/reprints.